# Second-harmonic generation enhancement in the presence of Tamm plasmon-polaritons

**B. I. Afinogenov, V. O. Bessonov, and A. A. Fedyanin***

*Faculty of Physics, Lomonosov Moscow State University, Moscow 119991, Russia*
**Corresponding author: fedyanin@nanolab.phys.msu.ru*

Received September 17, 2014; revised November 9, 2014; accepted November 13, 2014;
posted November 14, 2014 (Doc. ID 223240); published December 10, 2014

Resonant enhancement of second-harmonic generation (SHG) intensity from a thin metal film is demonstrated in a Tamm plasmon-polariton mode excited at a metal/photonic crystal interface using nonlinear spectroscopy. Nonlinear effects enhancement in proposed structures exhibit strong polarization dependence (1:200 for the orthogonal fundamental polarizations). SHG enhancement factor evinces considerable angular dependence, rising from 50 for the 45° angle of incidence to 170 for the 10° angle of incidence. The results are analyzed numerically using a nonlinear transfer matrix technique. The findings elucidate the potential of Tamm plasmon-polaritons in the nonlinear optical applications. 

*OCIS codes:* (350.4238) Nanophotonics and photonic crystals; (190.4350) Nonlinear optics at surfaces; (250.5403) Plasmonics.
http://dx.doi.org/10.1364/OL.39.006895

The Tamm plasmon-polariton (TPP) is the surface electromagnetic mode at the interface between a one-dimensional photonic crystal (PC) (distributed Bragg reflector) and a metal film [1,2]. TPPs exhibit a parabolic in-plane dispersion law lying inside the light cone [3]. Therefore, in contrast to surface plasmon-polaritons [4] and electromagnetic surface waves [5,6], which require prism or grating-coupling schemes, TPPs can be generated by direct optical illumination. Experimentally, TPPs manifest themselves as sharp resonances in reflection and transmission spectra. The spectral position of TPPs can be tuned inside the photonic bandgap by varying the thickness of the topmost layer of a PC bound to a metal film [7]. Over the past several years, TPPs have become a new area of study in the field of optics due to their interesting properties and due to the simplicity in the design and fabrication of TPP-supporting structures. Strong couplings of TPPs to excitons [8,9], microcavity modes [10], and surface plasmon-polaritons [11] have been demonstrated. The possibility of confining and tailoring TPP modes through structuring metal films [12] has been used to fabricate vertical-cavity compact lasers [13,14] and integrated circuits [15].

Optical second-harmonic generation (SHG) is a powerful noninvasive tool used to study surfaces and optically accessible buried interfaces in condensed matter systems possessing cubic or isotropic symmetry [16]. Dipole SHG is forbidden in the bulk of these centrosymmetric materials, and the main part of the second-harmonic (SH) signal is generated at surfaces and interfaces with broken inversion symmetry. The proportionality of the SH intensity to the square of the fundamental field intensity results in a high sensitivity of the SHG to the electromagnetic field localization inside micro- and nanostructures. SHG has been used as a probe of the field localization of the defect modes of single [17,18] and coupled [19,20] planar microcavities. Many metals, e.g., silver and gold, are centrosymmetric, and almost the entire SH signal is generated in few atomic layers of metal film surfaces [21]. Thus, TPP-induced electromagnetic field localization at a metal/PC interface can be probed by SHG from the nanometer-thick buried boundary of the metal film. Impact on the optical harmonics generation due to electromagnetic field enhancement in localized and surface plasmons have been extensively studied theoretically and experimentally [22]. Several theoretical investigations were also performed to shed light on the influence of the TPP excitation on the enhancement of the nonlinear optical effects in PC/metal structures [23].

In this Letter, we present experimental evidence for electromagnetic field localization at the buried interface of a metal film and a PC at the TPP resonance using a nonlinear-optical probe. It is shown that the emergence of the TPP in a metal/PC structure leads to an enhancement in the SHG intensity from the thin metal film by a factor of up to 170. A series of experiments using various polarization combinations reveals the polarization properties of the SH radiation generated in the sample.

The investigated distributed Bragg reflector samples consisted of six pairs of $ZrO_2/SiO_2$ layers with thicknesses of 110 and 145 nm. The layers were deposited onto a fused quartz substrate via thermal evaporation. Because the spectral position of the TPP depends on the thickness of the PC layer bound to the metal film, the thickness of the topmost layer of the PC was adjusted to 220 nm to tune the TPP spectral position to 800 nm under normal incidence. The photonic bandgap (PBG) of the resulting structure is spectrally located between 700 and 1050 nm [Fig. 1(a)]. The distribution of the electromagnetic field at wavelengths inside the PBG is characterized by an exponential decay into the PC, as shown in Fig. 1(c). For excitation of the TPP, the PC was covered by a semi-transparent 30-nm-thick gold film, allowing for measurements in transmission geometry. The corresponding distribution of the electromagnetic field in a PC/Au sample at the TPP resonance is shown in Fig. 1(d). In contrast to the case of a bare PC, the electromagnetic field distribution exponentially grows into the PC, with the magnitude increasing 16-fold in the last layer. A relatively small number of periods were purposely selected to obtain sufficient localization of the electromagnetic field in the TPP mode. Two reference samples were also prepared: a bare PC without gold and a 30-nm-thick gold film on a fused silica substrate.

 

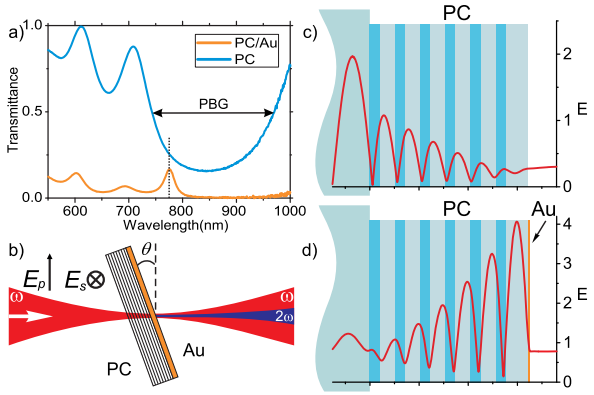


Fig. 1. (a) Transmittance spectra of a PC (top blue curve) and the PC/gold structure (bottom orange curve). The angle of incidence is $\theta = 20°$. (b) Schematic of the SHG experiment. $E_p$ and $E_s$ indicate orientation of the electric field vector for $p$ and $s$ polarization, respectively. (c), (d) Numerical calculation of the electric field distribution in the PC (c) and in a PC/Au structure (d) at 770 nm, corresponding to the dotted line in (a). Electric field is normalized by the incident. Radiation is incident from the left.

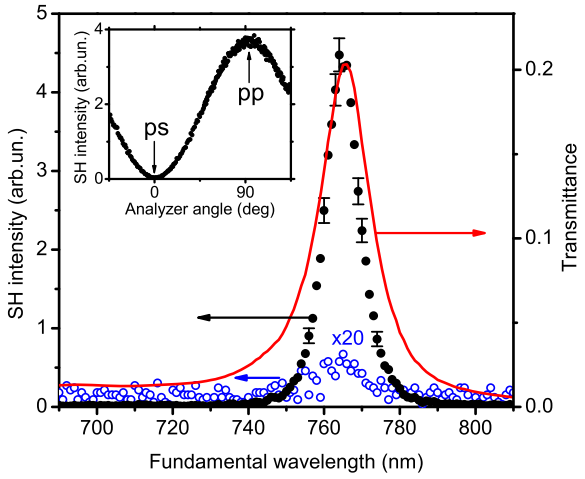


Fig. 2. Curve is the experimental transmittance spectrum of the PC/Au sample. The solid circles show the experimental SHG spectrum of the PC/Au sample using the $pp$ polarization combination. The open circles represent the experimental SHG spectrum of the PC/Au sample using the $ps$ polarization combination multiplied by 20. The inset shows the dependence of the SH intensity at 768 nm on the analyzer angle.

A Ti:sapphire oscillator was used as the source of the fundamental radiation, providing 130-fs pulses with an 80-MHz repetition rate. The fundamental wavelength was tuned from 700 to 820 nm. Two Glan–Taylor laser prisms were used to control the power and polarization of the fundamental beam. The incident light was focused on a 40-μm-wide spot in the sample [Fig. 1(b)], with a pump power density of 1 GW/cm$^2$. The sample was PC-faced to the fundamental beam to prevent SH interference in the PC. The SH radiation, generated via transmission through the sample geometry, was collimated, and its polarization state was analyzed using a Glan–Taylor laser prism. The analyzer was mounted on a motorized rotation stage, which enabled the analyzer angle to be set with an accuracy of 0.005°. Then, the SH beam passed through a 9-mm-thick BG39 filter to reject the fundamental light and was detected using a photomultiplier tube connected to a gated photon counter, with each point being recorded for 20 s. The measurements of the transmittance spectra were performed simultaneously with the SHG measurements to provide control over the TPP excitation. The experiment was performed using various polarization combinations of the fundamental and SH radiation. To measure the angular dependence of the SH intensity, the sample was mounted on a motorized rotation stage.

Figure 2 presents the transmittance spectrum of the PC/Au sample measured at a 20° angle of incidence. A sharp peak associated with the TPP excitation is observed near 768 nm. The transmittance around the peak is low because the complete spectral region shown in the figure corresponds to the photonic bandgap of the PC. The black circles represent the SHG spectrum of the PC/Au sample for the $pp$ combination of the fundamental and SH radiation polarizations. The spectrum also exhibits a resonance near 768 nm. The SH intensity at the maximum of the peak is 240 times larger than the intensity level far from the resonance. The peak intensity was also measured as a function of the analyzer angle for the given $p$ polarization of the fundamental beam (inset in Fig. 2). The strong polarization dependence of the SH signal was observed to exhibit the maximum using the $p$-polarized SH ($pp$ combination) and the minimum using the $s$-polarized SH ($ps$ combination). SHG spectra were also measured for the reference samples. The fundamental light intensity in these cases was increased 30-fold to emphasize weak nonlinear effects. Neither spectrum exhibited resonance features in the investigated spectral region; however, the intensity of the SH generated by the PC is at least three orders of magnitude smaller than the SH intensity from the gold film. Thus, the nonlinearity of the investigated PC/Au sample is primarily determined by the nonlinearity of the gold film. In the case of TPP excitation, the electromagnetic field is localized at the interface between the metal and the PC. Because the major contribution to the SHG comes from the metal surface, the enhancement of the local electromagnetic field leads to the enhancement of the SHG from the PC/Au sample. The enhancement factor is 120 in comparison with the SHG from the 30-nm-thick gold film.

Experiments were also performed with other combinations of the fundamental and SH radiation polarizations. The SHG spectrum for the $ps$ combination is shown in Fig. 2. This spectrum is magnified by a factor of 20 to emphasize the faint peak in the spectral region of the TPP resonance. The magnitude of the SHG resonance is 200 times less than that for the $pp$ combination. For the $sp$ and $ss$ polarization combinations, the SHG resonance is of the same intensity as that for the $ps$ polarization combination. This result suggests that hyper Rayleigh scattering [24] is a dominating factor of the SHG in forbidden polarization combinations due to the nanoroughness of the metal film.

Figure 3 shows the SH intensity spectra when the angle of incidence of the fundamental light was varied from 10° to 45° with a step size of 5°, measured using the $pp$ combination of polarizations normalized to the

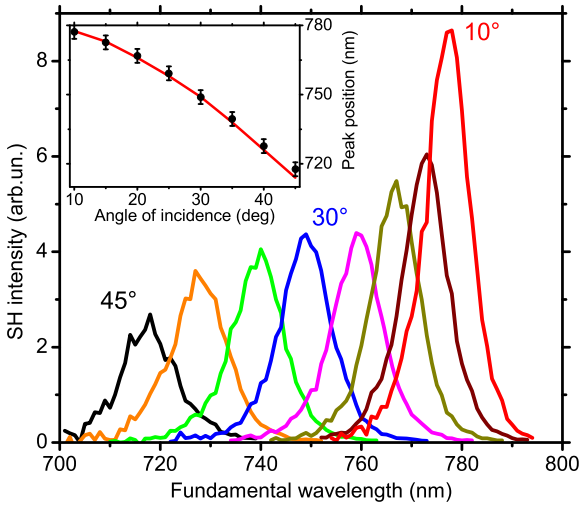


Fig. 3. SH intensity spectra for the angle of incidence of the fundamental radiation tuned from 10° to 45° with a step size of 5°. All spectra are measured using the *pp* combination of the fundamental and SH radiation polarizations. The inset shows the measured spectral position of the SHG resonance versus the angle of incidence of the fundamental light with dots and the TPP dispersion law with a solid curve.

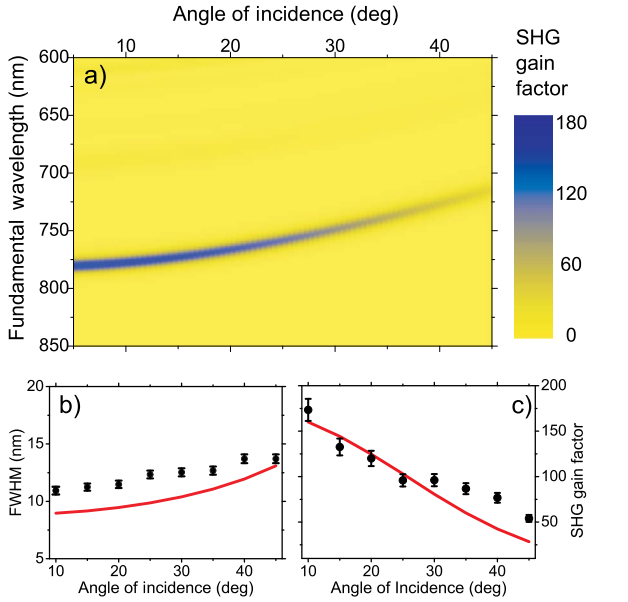


Fig. 4. (a) Image plot of the SHG enhancement factor versus angle of incidence and wavelength of the fundamental radiation. (b) Experimental (dots) and calculated (curve) FWHM of the SHG resonance as a function of the angle of incidence of the fundamental light. (c) Experimental (dots) and calculated (curve) SHG enhancement factor as a function of the angle of incidence of the fundamental light.

corresponding SH intensity spectra of the 30-nm-thick gold film. Because the TPP resonance blue shifts as the angle of incidence increases, the SHG resonance shifts to shorter wavelengths. A gradual decrease in the SH intensity and an increase in the resonance width can be observed as the angle of incidence increases. The inset in Fig. 3 shows the experimental spectral position of the SHG resonance as a function of the angle of incidence of the fundamental light and the calculated dispersion curve of the TPP. They coincide, which confirms that the SHG enhancement is TPP induced. SH intensities from both PC/Au sample and bare Au film fall toward zero with the decrease of the angle of incidence. After normalization, it results in a 0/0 uncertainty, therefore, considering a slight angular divergence, no SHG spectra were measured for angles of incidence below 10°.

Numerical calculations were performed using the nonlinear transfer matrix method [25] to analyze the SHG enhancement in the presence of the TPP. The parameters of the model structure were the same as those of the experimental sample. The dispersion of the optical parameters of the materials was taken from Refs. [26–28]. The second-order nonlinear susceptibility tensor of gold, $\hat{\chi}^{(2)}$, was constructed using the data from Ref. [21]. The roughness of the metal was not considered, and hyper Rayleigh scattering contributions to the SHG were neglected; thus, no *ps*, *sp* or *ss* signal was obtained in the calculated spectra.

The numerical results of the angular dependence of the SHG spectra using the *pp* polarization combination are shown in Fig. 4(a). This figure shows the SH intensity generated by the PC/Au structure divided by the SH intensity generated by the Au film versus the angle of incidence and versus the fundamental light wavelength. The dark stripe coincides well with the TPP dispersion curve and corresponds to the TPP-induced SHG resonance. The maximum enhancement is obtained at the near-normal incidence, peaking at 200. Figure 4(b) shows the dependence of the full width at half-maximum (FWHM) of the measured (dots) and calculated (curve) SHG resonances on the angle of incidence of the fundamental radiation. The trend of the monotonic increase in the FWHM with an increase in the angle of incidence can be observed. However, the measured resonance line shape is slightly wider than the calculated one. Figure 4(c) presents the SHG enhancement factor versus the angle of incidence of the fundamental light. As the angle of incidence increases, both the experimental (dots) and calculated (curve) SHG enhancement factors monotonically decrease from 170 for $\theta = 10°$ to 50 for $\theta = 45°$. The behavior of the experimental SH intensity profiles is in very good agreement with the calculated behavior. The inexact correspondence is most likely caused by the angular divergence of the fundamental radiation, the finite width of the fundamental pulse spectrum, and the stretching of the focal spot due to the rotation of the sample.

In conclusion, experimental proof of SHG enhancement in a one-dimensional PC terminated by a semi-transparent gold film in the presence of a Tamm plasmon-polariton is obtained. A TPP-induced 170-fold enhancement in the SH intensity in comparison with the SHG from the gold film is observed. The effect is the strongest for the *pp* combination of the fundamental and SH radiation polarizations. As the angle of incidence increases, the SHG resonance shifts to shorter wavelengths, decreases in amplitude, and increases in width. The proposed nonlinear-optical technique is promising for investigating the local field distribution at buried interfaces in structures with active layers. This technique can also be used to create maps of thicknesses in samples with metal layers.

This work was supported in part by the Russian Foundation for Basic Research.

**References**


1. J. A. Gaspar-Armenta and F. Villa, J. Opt. Soc. Am. B **20**, 2349 (2003).
2. A. P. Vinogradov, A. V. Dorofeenko, S. G. Erokhin, M. Inoue, A. A. Lisyansky, A. M. Merzlikin, and A. B. Granovsky, Phys. Rev. B **74**, 045128 (2006).
3. M. Kaliteevski, I. Iorsh, S. Brand, R. A. Abram, J. M. Chamberlain, A. V. Kavokin, and I. A. Shelykh, Phys. Rev. B **76**, 165415 (2007).
4. H. Raether, *Surface Plasmons on Smooth Surfaces* (Springer, 1988).
5. W. M. Robertson and M. S. May, Appl. Phys. Lett. **74**, 1800 (1999).
6. I. V. Soboleva, E. Descrovi, C. Summonte, A. A. Fedyanin, and F. Giorgis, Appl. Phys. Lett. **94**, 231122 (2009).
7. M. Sasin, R. Seisyan, M. Kaliteevski, S. Brand, R. Abram, J. Chamberlain, I. Iorsh, I. Shelykh, A. Egorov, A. Vasilev, V. Mikhrin, and A. Kavokin, Superlattices Microstruct. **47**, 44 (2010).
8. M. Kaliteevski, S. Brand, R. A. Abram, I. Iorsh, A. V. Kavokin, and I. A. Shelykh, Appl. Phys. Lett. **95**, 251108 (2009).
9. C. Symonds, A. Lemaître, E. Homeyer, J. C. Plenet, and J. Bellessa, Appl. Phys. Lett. **95**, 151114 (2009).
10. R. Brückner, M. Sudzius, S. I. Hintschich, H. Fröb, V. G. Lyssenko, and K. Leo, Phys. Rev. B **83**, 033405 (2011).
11. B. I. Afinogenov, V. O. Bessonov, A. A. Nikulin, and A. A. Fedyanin, Appl. Phys. Lett. **103**, 061112 (2013).
12. O. Gazzano, S. M. de Vasconcellos, K. Gauthron, C. Symonds, J. Bloch, P. Voisin, J. Bellessa, A. Lemaître, and P. Senellart, Phys. Rev. Lett. **107**, 247402 (2011).
13. C. Symonds, G. Lheureux, J. P. Hugonin, J. J. Greffet, J. Laverdant, G. Brucoli, A. Lemaître, P. Senellart, and J. Bellessa, Nano Lett. **13**, 3179 (2013).
14. R. Brückner, A. A. Zakhidov, R. Scholz, M. Sudzius, S. I. Hintschich, H. Fröb, V. G. Lyssenko, and K. Leo, Nat. Photonics **6**, 322 (2012).
15. T. C. H. Liew, A. V. Kavokin, T. Ostatnický, M. Kaliteevski, I. A. Shelykh, and R. A. Abram, Phys. Rev. B **82**, 033302 (2010).
16. Y. R. Shen, Nature **337**, 519 (1989).
17. J. Trull, J. Martorell, R. Corbalán, and R. Vilaseca, Opt. Lett. **20**, 1746 (1995).
18. V. Pellegrini, R. Colombelli, I. Carusotto, F. Beltram, S. Rubini, R. Lantier, A. Franciosi, C. Vinegoni, and L. Pavesi, Appl. Phys. Lett. **74**, 1945 (1999).
19. T. V. Dolgova, A. I. Maidykovski, M. G. Martemyanov, A. A. Fedyanin, O. A. Aktsipetrov, G. Marowsky, V. A. Yakovlev, and G. Mattei, Appl. Phys. Lett. **81**, 2725 (2002).
20. D. G. Gusev, I. V. Soboleva, M. G. Martemyanov, T. V. Dolgova, A. A. Fedyanin, and O. A. Aktsipetrov, Phys. Rev. B **68**, 233303 (2003).
21. D. Krause, C. W. Teplin, and C. T. Rogers, J. Appl. Phys. **96**, 3626 (2004).
22. S. Kim, J. Jin, Y.-J. Kim, I.-Y. Park, Y. Kim, and S.-W. Kim, Nature **453**, 757 (2008).
23. K. J. Lee, J. W. Wu, and K. Kim, Opt. Express **21**, 28817 (2013).
24. O. A. Aktsipetrov, A. A. Fedyanin, T. V. Murzina, G. P. Borisevich, and A. A. Kononenko, J. Opt. Soc. Am. B **14**, 771 (1997).
25. D. S. Bethune, J. Opt. Soc. Am. B **6**, 910 (1989).
26. P. B. Johnson and R. W. Christy, Phys. Rev. B **6**, 4370 (1972).
27. I. H. Malitson, J. Opt. Soc. Am. **55**, 1205 (1965).
28. D. L. Wood and K. Nassau, Appl. Opt. **21**, 2978 (1982).